Chapter IV

Ultrastructure of *Treponema primitia* by electron cryotomography

Gavin E. Murphy[1], Eric G. Matson[2], Jared R. Leadbetter[2],

Howard C. Berg[3], Grant J. Jensen[1*]

Divisions of Biology[1] and Environmental Science and Engineering[2], California Institute of Technology, Pasadena, CA 91125,

Department of Molecular and Cellular Biology, Harvard University, Cambridge, MA 02138[3]

*To whom correspondence should be addressed: 1200 E. California Blvd., Pasadena, CA 91125, 626-395-8827 (phone), 626-395-5730 (fax), **Jensen@caltech.edu**.

Abstract

Members of the bacterial Phylum *Spirocheates* are generally spiral or undulate cells propelled by periplasmic flagella. The spirochete *Treponema primitia* is of particular interest because of its mutualistic role in the termite gut, where it is believed to cooperate with H_2-producing, cellulose-decomposing protozoa in the biotechnologically interesting process of converting wood into bioenergy. Here we report the ultrastructure of *T. primitia* as obtained by electron cryotomography of intact, frozen-hydrated cells. Several novel external structures were revealed including bowl-like objects decorating the outer membrane, arcades of hook-like filaments winding along the exterior, and tufts of fibrils extending from the cell tips. Inside the periplasm, cone-like structures were found at each pole. Instead of the single peptidoglycan layer typical of other Gram-negative bacteria, two distinct periplasmic layers were observed. These layers formed a central open space that contained two flagella situated adjacently to one another. In some areas, the inner membrane formed flattened infoldings that protruded into the cytoplasm. Within the cytoplasm were spherical granules, ribosome-like particles, chemoreceptor arrays, and a distinct nucleoid region. High-speed light microscopic images of swimming *T. primitia* cells showed that cell bodies remained rigid and moved in a helical rather than planar motion. These movements and ultrastructural details support the particular model for spirochete motility that posits rotation of the outer sheath with respect to the protoplasmic cylinder. The wealth of ultrastructural detail seen here by electron cryotomography suggests that there may be more complexity and diversity in bacterial ultrastructure than has yet been appreciated.

Introduction

Many members of the phylum *Spirochaetes*—such as *Treponema pallidum*, *Leptospira interrogans* and *Borrellia burgdorferi*—are important human pathogens, causing the diseases syphilis, Weil's disease, and Lyme disease, respectively. Others, however, cooperate beneficially with their animal hosts. *Treponema primitia,* for example, is a species that inhabits the hindgut of the termite *Zootermopsis angusticolis* and synthesizes acetate from H_2 and CO_2, which are intermediates generated by gut protozoa during the fermentation of wood polysaccharides. Acetate serves as the major energy source of their insect host, and up to a third of it is derived from CO_2-reducing homoacetogens like *T. primitia* [1-3]. In early microscopic studies on termite gut ecosystems, spirochetes were observed to attach to, and sometimes even propel, certain hindgut flagellate protozoa [4-6]. It has since been hypothesized that that interspecies H_2-transfer between H_2-producing protozoa and H_2-consuming spirochetes such as *T. primitia* might be promoted by such associations [4].

Spirochetes are unusual with respect to other bacteria in that their flagella are confined within the periplasm. This feature has led to the biophysical question: How do internally situated flagella impart cell motility? Rotation of periplasmic flagella is thought to drive motility by causing the entire cell body to gyrate and/or rotate [7-12]. Compared to externally flagellated bacteria, spirochetes move effectively in gel-like, viscous environments [13, 14]. Motility and its enabling ultrastructure has been linked to spirochete pathogenesis [15] and in *T. primitia*, both are likely to be important for inhabiting the termite gut.

Most of what is known about spirochete cell structure comes from conventional EM studies, which involve chemical fixation, dehydration, plastic-embedding, sectioning, and heavy metal staining. While some details are lost or distorted by these procedures, they have revealed inner and outer membranes, subterminally attached periplasmic flagella, and close associations with host protozoa [6]. More recently, it has become possible to image intact cells in three dimensions (3-D) in a nearly native state by electron cryotomography (ECT) [16, 17]. In this technique, cells are spread into thin films and frozen so quickly that ice crystals do not form, thus preserving the specimen in a life-like, "frozen-hydrated" state. A series of images is then recorded of each frozen cell as it is rotated incrementally in an electron microscope. The images are used to calculate a three-dimensional reconstruction of the entire cell and its contents with a resolution that is typically sufficient to identify and locate large macromolecular complexes *in-situ*. In this way, the first structure of a complete bacterial flagellar motor was obtained by imaging *T. primitia* cells [18]. Previous tomographic reconstructions of the spirochete *Treponema phagedenis* cells have already shown their interesting cytoskeletal architecture, although these cells were conventionally preserved rather than frozen-hydrated [19].

By imaging *T. primitia* cells in a frozen-hydrated state by ECT, several surprising ultrastructural features have been discovered including bowls, arches, and fibrils on the outer surface; a multi-layered and capped periplasmic space; and a subdivided cytoplasm with internal membrane sacs and other large structures. Together with high-speed, light microscopic video of swimming *T. primitia* cells, these ultrastructural features support the particular model of motility wherein the flagella cause rotation of a flexible outer

sheath about a rigid, helical, protoplasmic cylinder [11]. The features of *T. primitia* identified in this study also suggest that the complexity and diversity of bacterial ultrastructure may have been underestimated by previous imaging technologies.

Results

Examination of T. primitia *in the near-native state reveals novel ultrastructural features.*

Although *T. primitia* is an anaerobic organism that can survive for only a short time in the atmosphere, it is still a favorable specimen among spirochetes for high resolution ECT because it is thin and can be cultured relatively easily. *T. primitia* cells are fragile and tended to lyse when centrifuged or when blotted during the robotic vitrification process. To reduce this problem, cells were quickly frozen directly from their culture media using a manual blotting procedure that reduced trauma. Eighteen 3-D reconstructions were calculated that together included one complete cell and twenty-three magnified cell tips. Three of these cells were intact but the others had ruptured outer membranes on one side of the cell. The different cell reconstructions referred to below are numbered 1–7.

Fig. IV-1 shows a 10 nm thick, 700 nm long (~ 10% of the cell length) slice through the reconstruction of cell #1. Several novel features were observed, including structures we refer to as “surface bowls,” “surface hook arcades,” and "polar fibrils." A polar "cone" was seen inside the periplasm as well as the two expected flagella and flagellar motors. Ribosome-like particles were visible in the cytoplasm. Surface views of the manually segmented cell #1 are shown in Fig. IV-2 and Supp. Movie IV-S1.

Because samples can only be tilted to ~ 65˚, the resolution of the reconstructions is anisotropic, and surfaces parallel to the grid are difficult to resolve. Thus the tops and bottoms of the cell are missing in the segmentations. Nevertheless, the width of the cells perpendicular to the beam was ~ 350 nm. The flagella and hook arcades wrapped right-handed about the cell. The flagella from both poles were seen at this tip lying side-by-side beneath the surface hook arcade: the motor for the flagellum colored red was found ~ 100 nm away from the tip of the inner membrane, and the flagellum colored green (which emanated from the opposite cell pole) ended about 500 nm away.

Fig. IV-3 and Supp. Movie IV-S2 show similar surface views of cell #2, in which two cells were seen attached to each other. The cell in the lower half of the figure (#2b) was located in an ice-filled hole in the carbon supporting film, while the upper cell (#2a) lay on the carbon. Cell #2b's outer membrane was lysed, but #2a's was not. This happened several times, suggesting that the outer membrane was fragile, but it could be protected somewhat from the blotting and plunge-freezing procedure by the supporting carbon film. The side views (Fig. IV-3B and 3D) show how the carbon film apparently also pushed the cells slightly out of alignment. Other connected cells were observed in the light microscope and they were still motile.

Bowl-like structures arrayed the exterior surface of the outer membrane.

Novel "surface bowls" were present on the outer membranes of all the cells. While they usually appeared to be randomly arranged, in one case they formed 2 or 3 rows of right-handed helices (Fig. IV-3G). Sometimes the bowls were present underneath the surface hooks (Fig. IV-2B, 5A, and 5B). Fifty-six individual bowls were extracted, aligned,

averaged, and circularly symmetrized to produce a higher signal-to-noise density map (Fig. IV-4). The bowls were 16 nm high, 45 nm wide, and their bottoms were 8 nm above the membrane (measured from the center of each feature). In the symmetrized average the membrane just below the bowl appeared "dimpled," probably because the point-spread function of the microscope produces an inverse halo around dense objects. In this case, the halos around the bowl and the membrane are expected to slightly reduce the apparent density of the top of the membrane, the bottom of the bowl, and the "stalk" that connects them.

Arcades of counter-opposing hook-like structures lined the surface.

Long series of arches (arcades) were seen decorating the outside of eighteen of the twenty-four partially- or fully-reconstructed cells, including both lysed or unlysed cells. In cell #1, an arcade began over the motor and apparently wrapped right-handed around the cell directly above the flagella along the entire reconstructed region (Fig. IV-2, and panel B in particular). There were four arcades on cell #2a and a partial arcade on cell #2b. A pair of arcades ran above cell #2a's flagella, but it did not wrap directly over them (Fig. IV-3D–G). Another arcade was located a quarter arc from the pair, and the fourth was located opposite the pair. Fig. IV-5 highlights a particularly well-reconstructed pair of ~ 600 nm long arcades that ran atop lysed cell #3. The possible relationship between the arcades and the flagella was puzzling. In many cases there were arcades on cell surfaces far away from the flagella, and most of the flagella were not covered by arcades, but there were a few stunning instances where the hook arcades were seen directly over the flagella for long distances, as if they were associated (as in cell #1).

The arches appeared to be composed of two symmetric hooks that joined at the top. Several sections of a hook arcade were aligned together and averaged, then positioned onto their probable two-fold symmetry axis and symmetrized. The two-fold symmetrized average (Fig. IV-5D) shows the meeting of individual hooks at the top, where adjacent arches touched each other to form a continuous roof. The pillar area did not emerge from the averaging because the density was weak and apparently non-uniform. The arches were seen to be angled 35˚ from the long axis of the arcade, so that each hook abutted the one two positions away from it at the base (Fig. IV-5E). The hooks were ~ 4 nm wide; the pillars were 29 nm apart, and the arcades were 40 nm wide and 43 nm high.

Polar fibrils projected from the cell tips.

Tufts of 6 nm thick fibrils extended from the tips of twenty-two of the cells (Fig. IV-6), including both poles of cell #6 (Fig. IV-6G). Some tips had one tuft (Fig. IV-3, Fig. IV-6 A-D and G), others two (Fig. IV-2 and 6E), and still others were forked (Fig. IV-6H). Some fibrils were short and fairly straight and others were long and curved, but it is unclear whether they were fundamentally different. The longest straight fibril was 350 nm and the shortest curvy fibril was 370 nm, so perhaps beyond a certain persistence length they bend. Both types were sometimes seen bundled together in the same tuft. An exceptional 1.6 micrometer long fibril was seen on cell #1 (Fig. IV-6E). In some cases, density could be traced from the fibrils through the periplasmic cone all the way to the inner membrane (Fig. IV-6C).

Cone-shaped material occupied the periplasmic poles.

Cone-shaped, apparently porous, periplasmic structures were present at the tips of all but one of the reconstructed cells (Fig. IV-7 and Supp. Movie IV-3). The cones lay underneath the outer membrane region from which the fibrils extended. In the two reconstructions of connected cells, each cell had its own periplasmic cone, and the two cones abutted tip-to-tip. Since these densities were still cone-shaped, even in connected cells where the outer membrane did not limit them (Fig. IV-7C), the conical shape is probably inherent to the structure rather than imposed by the outer membrane.

Periplasmic flagella lay between two distinct periplasmic cell wall layers.

Two clear layers were visible between the inner and outer membranes in some reconstructions (Fig. IV-8A and Supp. Movie IV-S4). In order to confirm this visual observation, density profiles along normals to the surface (like "core samples") were calculated and averaged in regions where the periplasm was approximately uniformly thick (Fig. IV-8E). This excluded the area around flagella and especially the flagellar motor, where the periplasm was wider (also visible in Fig. IV-1A). Four peaks emerged, corresponding, respectively, to the outer membrane at the top/origin, an “outer periplasmic layer” 9 nm below, the “inner periplasmic layer” 12 nm deeper, and finally the inner membrane another 7 nm lower. Densities were measured as a function of distance from the outer membrane, so structural variability increasingly blurred features towards the interior. This is why the peaks corresponding to the inner membrane and inner periplasmic layers are broader than their outer counterparts. The flagellum was 20

nm thick and in some views was clearly seen to lie between the two periplasmic layers, pushing them apart (see also Supp. Movie IV-4).

Cytoplasmic structures

Flattened membrane sacs were visible in several reconstructed cells. They were always close to the inner membrane and appeared to be membrane invaginations (Fig. IV-9). Spherical bodies ~ 30 nm wide with smooth and uniform internal textures reminiscent of polymer storage granules were seen in the cytoplasm of several of the cells (Fig. IV-7C). Strips of density resembling chemotaxis receptor arrays were present ~ 20 nm from the inner membrane close to flagellar motors at the cell poles (Fig. IV-9A) [20, 21]. In all the reconstructions the cytoplasm was divided into two regions with different textures: a more punctuated, cylindrical shell on the outside filled with ribosome-like particles; and a smoother, inner tube roughly half the diameter of the inner membrane (~ 125 nm) without ribosome-like particles. The inner tube was likely the nucleoid region that houses the genome (Fig. IV-9A).

T. primitia *appeared to be a rigid helix as it swam.*

High-speed movies were recorded of cells swimming in a buffered salt solution containing 0.175% methyl cellulose (viscosity = 4 cP), which is only slightly more viscous than water (Fig. IV-10 and Supp. Movie IV-5). Because motility models for other spirochetes such as *Leptospira* and *Borrelia* involve cell shape changes and/or planar waves, we looked carefully for evidence of these possibilities. *T. primitia* cells looked like rigid helices at all times, and no evidence of polar hooks or gyrations was

seen. Projections of planar-wave-shaped cells like *Borrelia* appear as straight lines and then later as sine waves of varying amplitude as the plane of the wave rotates in and out of the projection direction. Here, the cells always appeared sinusoidal with constant amplitude, consistent with a rigid helical rotation. Further, the relative height of each section along the cell was discernable by the sharpness of its focus. Again, unlike a planar cell but consistent with a rigid helix, points of similar focus were seen to move steadily down the cell (arrowheads, Fig. IV-10). The helical pitch (wavelength) of the cell was ~ 2.5 μm; the radius was ~ 0.6 μm, and the cell moved at ~ 12 μm/s. In Fig. IV-10, it can be seen that a complete helical revolution occurred every ~ 60 ms (i.e., the shape is nearly identical at 0 and 60, 10 and 70, 20 and 80 ms), but the cell translated just ~ 0.7 μm, or 29% of a wavelength, per revolution. Thus there was substantial circumferential slip, as expected for propulsion in a dilute aqueous medium. For comparison, *E. coli* swims at 30 μm/s in aqueous solutions [22].

Discussion

The ultrastructure of *T. primitia* was examined here using electron cryotomography and the results are summarized in Fig. IV-11A. Unique surface bowls dotted the outer membrane exterior. Novel hook-shaped appendages were aligned in parallel, face-to-face rows, generating macromolecular arcades striping the length of the cell's OM—sometimes, but not always, directly above the two juxtaposed periplasmic flagella. Fibrils extended from the cell tips. Periplasmic cones were found at the cell poles between the two membranes, and the flagella lay between two distinct periplasmic

layers. Cytoplasmic structures like membrane invaginations, chemotaxis strips and ribosome-excluded zones were visible.

In other organisms, familiar surface structures like S-layers, fimbriae, and fibrils serve as protective coats, as platforms for adhesion and interaction with neighbors and hosts, and in motility [23, 24]. The surface bowls and hook arcades seen here may perform similar functions. A "goblet" structure slightly taller and narrower than the surface bowls was seen to coat the outer membrane of *Flexibacter polymorphus* [25, 26]. However, the incomplete coverage of the surface bowls argues against a protective role. The positioning of some hook arcades over the flagella suggests a potential role in motility.

Symbiotic spirochetes are already known to use their cell tips to attach to protozoa [4, 6]. The fibrils seen here might similarly attach *T. primitia* to its protozoan hydrogen supplier. Most fibrils are known to extend from the outer membrane, but some originate from the inner membrane [27]. Here some fibrils were seen to extend into and perhaps all the way through the periplasmic cones, which may serve as anchor points for cell attachment or stabilizers for the poles during motility.

Normally gram-negative bacteria have only one peptidoglycan layer linked to proteins from both the outer and inner membrane. The unique motility strategy of spirochetes, however, presents a structural challenge because the rotation of the periplasmic flagella introduces unusual forces. If there were only one periplasmic layer in spirochetes, the flagella would have to rotate between the outer membrane and peptidoglycan layer, producing two potential problems: at least some of the outer membrane would be unsupported by peptidoglycan, and the forceful rotation of the

flagella might rupture the outer membrane. The discovery of two periplasmic layers in *T. primitia* offers an elegant solution. The flagella rotate within an apparently structurally reinforced space, and the whole outer membrane is supported. The inner periplasmic layer probably consists of peptidoglycan, since MotB of the flagellar stators (which is present in *Treponema*) is known to bind to peptidoglycan for stability [28]. The composition of the outer periplasmic layer is unknown, but the presence of such a layer may help explain the formation of patterns seen previously in the outer membranes of the related species S. *aurantia*, *S. litoralis*, and *T. microdentium* [6].

Spirochete motility is complex. Two classes of motility models exist, but only one of them is consistent with our observations of *T. primitia*. The first class is for spirochetes like *Leptospira interrogans* and *Borrelia burgdorferi*, for which the periplasmic flagella (PF) are stiffer than the "protoplasmic cylinder" (PC) [7, 8, 10, 12]. For *T. primitia,* the PC includes the inner membrane and the inner periplasmic layer. The second class is for spirochetes like *Cristispira balbianii* and *Spirocheta aurantia,* where the PF are less stiff than the PC [11, 13]. In both models, the PF rotate in place relative to the PC, because they are tethered to the PC. In the first model, bending and changes in the shape of the PC, i.e., propagation of a helical wave for *L. interrogans* and propagation of a planar wave for *B. burgdorferi*, are driven by the rotation of the PF. In the second model, the PC remains rigid but the whole cell is made to roll about the body axis by circumferential flow of the "outer sheath" (OS), which for *T. primitia* includes the outer membrane and the outer periplasmic layer. Since *T. primitia* appears to maintain a constant helical shape, only the second model is viable.

The flagellar motors at opposite ends of the cell are opposed, so when the PF rotate in opposite directions (one clockwise when viewed from outside the cell as it emerges from the inner periplasmic layer and the other counter-clockwise), they rotate in the same direction when viewed in transverse section (Fig. IV-11A). Friction between the PF and the OS causes the OS to rotate around the PC (counter-clockwise in Fig. IV-11B, as depicted by the brown arrow), and viscous shear between the OS and the external medium causes the entire cell (the PC and PF, and concomitantly, the OS) to roll in the opposite direction (clockwise, as depicted by the blue arrow in Fig. IV-11B and red arrows in Fig. IV-11C). If the body of the cell rolls clockwise and the PC is right-handed, this will cause the cell to drill (swim) into the page and to the upper right (as depicted by the straight green arrow in Fig. IV-11C). If the cell swims in a dilute aqueous medium rather than in a gel-like medium, thrust is generated by the slantwise slip of segments of the helical body relative to the external medium, just as thrust is generated by slantwise slip of segments of flagellar filaments for ordinary flagellated bacteria [29]. If the cell swims in a gel-like medium, e.g., 1% methylcellulose or dilute agar, it will bore its way through the medium like a corkscrew through a cork [13]. The medium used for the experiment shown in Fig. IV-10 by comparison is not nearly as gel-like and as expected, significant slippage was observed. In completing one revolution about its axis, this cell translated less than a third of its wavelength. In any event, if both flagellar motors change their directions of rotation, the cell will back up. If only one motor changes its direction of rotation, the cell will stop; and if the PC is sufficiently pliable, the cell might flex.

In the case of *T. primitia*, the OS did not appear to be wrapped tightly around the PC, consistent with this model in which the OS flows around the PC. Problems emerge, however, when reconciling the model with the ultrastructure. Hook arcades were seen over the flagella in the best-preserved cells. Counter rotation of the OS and PC (and its attached PF) would not permit alignment of the two except once per cycle. Also, counter rotation of the two membranes would presumably prevent efflux channels from forming. Efflux channels are either transitory or longer-lived alignments of inner and outer membrane channels and periplasmic adaptors to create “stovepipes” that expel cytoplasmic contents [30]. Sequence similarity using the Entrez database reveals that some efflux channels like NorM and AcrB, AcrA, and TolC are present in *Leptospira*, *Borrelia* and *Treponema* species (data not shown). If the OS and PC counter rotate, such channels would break. Also, if the fibrils connect to the periplasmic cone and inner membrane, then counter rotation would strain this connection.

These potential problems disappear if the OS does not move as a rigid body but instead flows and shears differently in different areas over the cell. The cone might stabilize the periplasm at the ends of the cell so that fibrils and efflux channels could assemble and function there. The cone would then not connect rigidly to the outer periplasmic layer, but rather "cap" it at the poles. The purpose of the outer periplasmic layer might be to roll over the flagella and support the outer membrane in the midcell region between the stable cones. The presumably fluid outer membrane would rotate with the outer periplasmic layer at the midcell, but move less at the cell poles above the cones, shearing as necessary in between to maintain its integrity. Perhaps the fragility of the OS, as exemplified by its lysis after blotting or mild centrifugation, is evidence of its

fluidity. In this scenario, the purpose of the hook arcade and surface bowls might be to enhance friction between the OS and the environment.

These hypotheses suggest specific experiments. The sequence of the *T. primitia* genome is nearing completion. The fibrils, surface bowls, and hook arcades should be identifiable as major components of purified outer sheaths. Once methods to introduce genetic alterations are established, deletion mutants may elucidate the functions of these structures. Single-molecule fluorescence experiments tracking tags on both the surface bowls or other external structure and simultaneously an inner membrane protein or the flagellum may confirm whether and where the OS rotates with respect to the PC. Fluorescent tags on efflux channels should reveal whether or not they are in fact confined to the poles. Overexpression of efflux channels might cause them to mislocalize to the midcell, linking the OS and PC there and disrupting motility. In any case, the remarkable structures seen here suggest that bacterial ultrastructure and motility may be more complex and diverse than anticipated.

Experimental Procedures

Cell Growth and Grid Preparation

Cultures of *T. primitia* strain ZAS-2 were grown at 23° C in sealed culture tubes containing 4YACo medium under an atmosphere of 80% H_2 and 20% CO_2 as described previously [3] and harvested during log-growth at an OD of ~ 0.6. To prevent aggregation in high-salt solutions, 10 nm colloidal gold was pretreated with 5% BSA for 30 minutes. It was then concentrated five-fold and 5 ml was applied to glow-discharged, carbon-coated R 2/2 quantifoil grids and dried. ZAS-2 is an obligate anaerobe but can

tolerate atmospheric conditions for about 20 minutes, so grids were frozen in small batches. A small volume of cell solution was removed with a syringe. 5 ml of the uncentrifuged solution was applied to a grid. When cells were centrifuged at a mild setting of 4000 x *g*, the outer membranes lysed, so centrifugation was avoided. Initially, grids were plunge frozen in liquid ethane on a Vitrobot (FEI Company) in 100% humidity using a 2 s blot time, a –2 offset, and a 1 s drain. Blotting on both sides of the grid by the Vitrobot caused catastrophic rupture of the outer membrane, so in order to minimize trauma, grids were manually blotted on the reverse side of the applied liquid and frozen using a gravity plunger.

Electron Tomography Data Collection and 3D Reconstruction

The data collection and reconstruction process was described previously [18]. Single-axis tilt series were collected using a 300 keV FEI Polara FEG TEM automated by UCSF Tomo [31]. Typically, tilts were incremented 1º from –63º to 63º. The magnification was 22,500 (0.98 nm/pixel) and the total dose was ~ 110 $e^-/Å^2$, distributed according to the 1/cos scheme. Tomograms were reconstructed using IMOD [32] and binned twofold (1.96 nm/pixel).

Image Processing

Reconstructions were segmented manually using Amira (Mercury Computing Systems). To display the fibrils, the region of the fibrils was segmented to create a mask, which was then applied to the volume file. The fibrils were displayed as an isosurface. Surface bowls and hooks were averaged by computationally extracting individual particles,

aligning, and averaging them using the Bsoft image processing package [33]. Two-fold symmetry was imposed on the surface hooks, and hundred-fold symmetry was imposed on the surface bowls to smooth the reconstructions. The true symmetry of the surface bowls, if any, is unknown. Amira was used to estimate all measurements. To measure periplasmic density, the volume of one cell interior to the outer membrane was segmented. A surface map was generated and then smoothed. Density normal to this one surface was measured at each vertex of the surface triangles using a customized Amira module. The density was averaged to display density versus periplasmic depth. Measurements were taken over more than 25,000 pixels, corresponding to about 1% of the total surface area of a cell.

Light Microscopy

Phase-contrast images of swimming cells were captured using a high speed AxioCamHS digital camera mounted on an AxioPlan 2 microscope (Carl Zeiss, Inc.).

Acknowledgements

We thank H. Jane Ding for creating an Amira module for analysis. This work was supported in part by NIH grants P01 GM66521 and R01 AI067548 to G.J.J., DOE grant DE-FG02-04ER63785 to G.J.J., a Searle Scholar Award to G.J.J., NSF grants DEB-0321753 and EF-0523267 to J.R.L., NIH grant AI016478 to H.C.B., NIH graduate fellowship F31 EB 004179 to G.E.M., and gifts to Caltech from the Ralph M. Parsons Foundation, the Agouron Institute, and the Gordon and Betty Moore Foundation.

References

1. Breznak, J. A., and Switzer, J. M. Acetate synthesis from H(2) plus CO(2) by termite gut microbes. *Appl Environ Microbiol*. **52**, 623-630 (1986).
2. Graber, J. R., Leadbetter, J. R., and Breznak, J. A. Description of *Treponema azotonutricium sp. nov*. and *Treponema primitia sp. nov*., the first spirochetes isolated from termite guts. *Appl Environ Microbiol*. **70**, 1315-20 (2004).
3. Leadbetter, J. R., Schmidt, T. M., Graber, J. R., and Breznak, J. A. Acetogenesis from H_2 plus CO_2 by spirochetes from termite guts. *Science*. **283**, 686-9 (1999).
4. Bloodgood, R. A., and Fitzharris, T. P. Specific associations of prokaryotes with symbiotic flagellate protozoa from the hindgut of the termite *Reticulitermes* and the wood-eating roach *Cryptocercus*. *Cytobios*. **17**, 103-22 (1976).
5. Cleveland, L. R., and Grimstone, A. V. The fine structure of the flagellate *Mixotricha paradoxa* and its associated micro-organisms. *Proc Roy Soc London*. **B159**, 668-686 (1964).
6. Holt, S. C. Anatomy and chemistry of spirochetes. *Microbiol Rev*. **42**, 114-60 (1978).
7. Goldstein, S. F., Buttle, K. F., and Charon, N. W. Structural analysis of the *Leptospiraceae* and *Borrelia burgdorferi* by high-voltage electron microscopy. *J Bacteriol*. **178**, 6539-45 (1996).
8. Goldstein, S. F., and Charon, N. W. Motility of the spirochete *Leptospira*. *Cell Motil Cytoskeleton*. **9**, 101-10 (1988).
9. Goldstein, S. F., and Charon, N. W. Multiple-exposure photographic analysis of a motile spirochete. *Proc Natl Acad Sci USA*. **87**, 4895-9 (1990).

10. Goldstein, S. F., Charon, N. W., and Kreiling, J. A. *Borrelia burgdorferi* swims with a planar waveform similar to that of eukaryotic flagella. *Proc Natl Acad Sci USA*. **91**, 3433-7 (1994).

11. Berg, H. C. How spirochetes may swim. *J Theor Biol*. **56**, 269-73 (1976).

12. Berg, H. C., Bromley, D. B., and Charon, N. W. Leptospiral Motility. *Symp Soc Gen Microbiol*. **28**, 285-294 (1978).

13. Berg, H. C., and Turner, L. Movement of microorganisms in viscous environments. *Nature*. **278**, 349-51 (1979).

14. Nakamura, S., Adachi, Y., Goto, T., and Magariyama, Y. Improvement in motion efficiency of the spirochete *Brachyspira pilosicoli* in viscous environments. *Biophys J*. **90**, 3019-26 (2006).

15. Li, C., Motaleb, M. A., Sal, M., Goldstein, S. F., and Charon, N. W. Gyrations, rotations, periplasmic flagella: the biology of spirochete motility in *The Spirochetes Molecular and Cellular Biology*. (Saier, M. H., Jr & Garcia-Lara, J., eds.), Horizon Press, Norfolk, (2001).

16. Jensen, G. J., and Briegel, A. How electron cryotomography is opening a new window into prokaryotic ultrastructure. *Curr Opin Cell Biol*. **in press** (2007).

17. Lucic, V., Forster, F., and Baumeister, W. Structural studies by electron tomography: from cells to molecules. *Annu Rev Biochem*. **74**, 833-65 (2005).

18. Murphy, G. E., Leadbetter, J. R., and Jensen, G. J. In situ structure of the complete *Treponema primitia* flagellar motor. *Nature*. **442**, 1062-4 (2006).

19. Izard, J., et al. Tomographic reconstruction of treponemal cytoplasmic filaments reveals novel bridging and anchoring components. *Mol Microbiol*. **51**, 609-18 (2004).

20. Lefman, J., et al. Three-dimensional electron microscopic imaging of membrane invaginations in *Escherichia coli* overproducing the chemotaxis receptor Tsr. *J Bacteriol*. **186**, 5052-61 (2004).

21. Zhang, P., et al. Direct visualization of receptor arrays in frozen-hydrated sections and plunge-frozen specimens of *E. coli* engineered to overproduce the chemotaxis receptor Tsr. *J Microsc*. **216**, 76-83 (2004).

22. Purcell, E. M. Life at low Reynolds number. *Am J Phys*. **45**, 3-11 (1977).

23. Fernandez, L. A., and Berenguer, J. Secretion and assembly of regular surface structures in Gram-negative bacteria. *FEMS Microbiol Rev*. **24**, 21-44 (2000).

24. Moissl, C., Rachel, R., Briegel, A., Engelhardt, H., and Huber, R. The unique structure of archaeal 'hami', highly complex cell appendages with nano-grappling hooks. *Mol Microbiol*. **56**, 361-70 (2005).

25. Ridgway, H. F. Ultrastructural characterization of goblet-shaped particles from the cell wall of *Flexibacter polymorphus*. *Can J Microbiol*. **23**, 1201-13 (1977).

26. Ridgway, H. F., Wagner, R. M., Dawsey, W. T., and Lewin, R. A. Fine structure of the cell envelope layers of *Flexibacter polymorphus*. *Can J Microbiol*. **21**, 1733-50 (1975).

27. White, D. *The Physiology and Biochemistry of Prokaryotes*. Oxford University Press, New York (2007).

28. Berg, H. C. The rotary motor of bacterial flagella. *Annu Rev Biochem.* **72**, 19-54 (2003).

29. Berg, H. C. *Random Walks in Biology*. Princeton University Press, Princeton (1993).

30. Piddock, L. J. Multidrug-resistance efflux pumps - not just for resistance. *Nat Rev Microbiol*. **4**, 629-36 (2006).

31. Zheng, Q. S., Braunfeld, M. B., Sedat, J. W., and Agard, D. A. An improved strategy for automated electron microscopic tomography. *J Struct Biol*. **147**, 91-101 (2004).

32. Kremer, J. R., Mastronarde, D. N., and McIntosh, J. R. Computer visualization of three-dimensional image data using IMOD. *J Struct Biol*. **116**, 71-6 (1996).

33. Heymann, J. B. Bsoft: image and molecular processing in electron microscopy. *J Struct Biol*. **133**, 156-69 (2001).

Supplementary material

The following supplementary material is available for this article:

Movie IV-S1. Segmented cell #1 with labeled components.

Movie IV-S2. Segmented cell #2 with labeled components.

Movie IV-S3. A focus on the periplasmic cones.

Movie IV-S4. Series of cross-sections through cell #8 showing two periplasmic layers.

Movie IV-S5. Light microscopy video of a single *T. primitia* cell swimming.

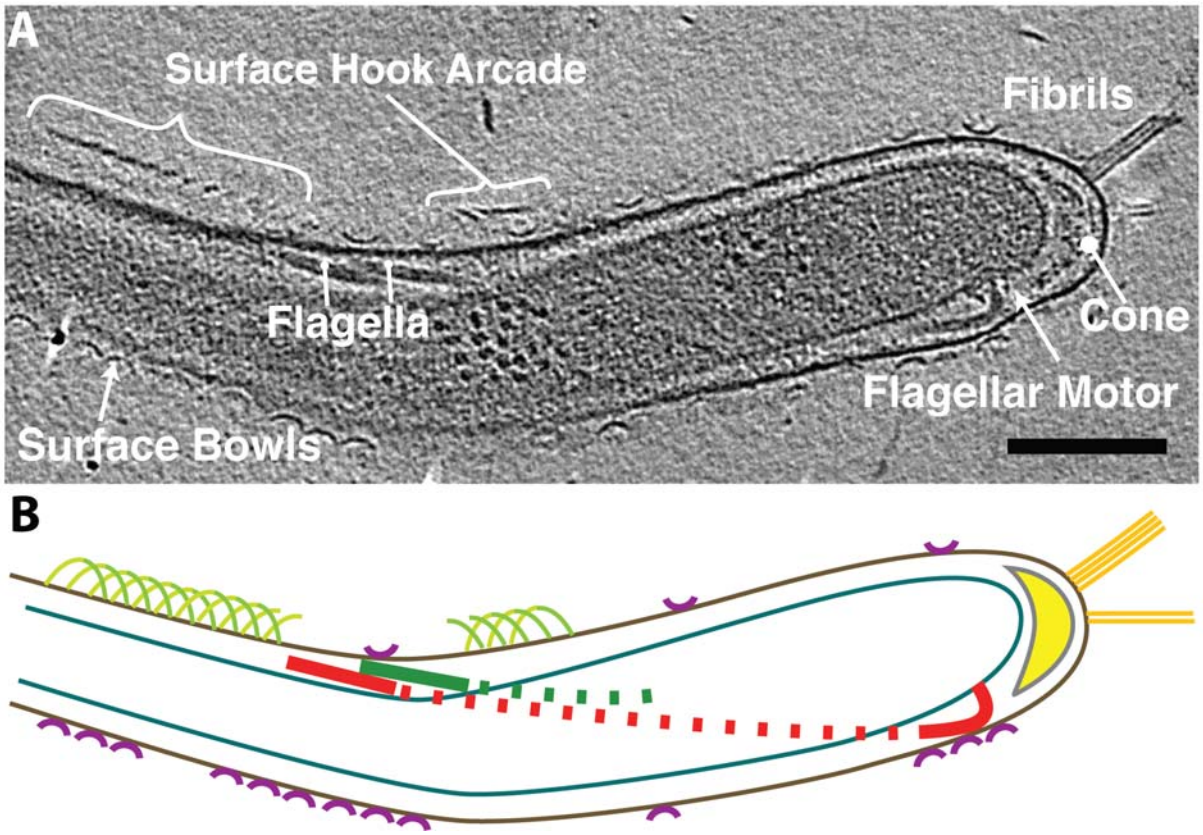

Fig. IV-1. Electron cryotomographic reconstruction of *T. primitia*

A. 10 nm section through the reconstruction of a frozen-hydrated *T. primitia* cell (cell #1). Surface bowls (magenta) dot the outer membrane surface. The surface hook arcades (chartreuse) wind atop the cell. Fibrils (orange) extend from the cell tip above a periplasmic cone (yellow). Periplasmic flagella (red and green) wrap around the cell. (Scale bar 200 nm.) B. Cartoon rendering of panel A. The same colors are used for all the figures and movies.

Fig. IV-2. Surface views of cell #1

A-D. Four side views of cell #1, incrementally rotated by 90˚. E. View of the cell tip showing the periplasmic cone underlying the fibrils. F. View from the midcell region.

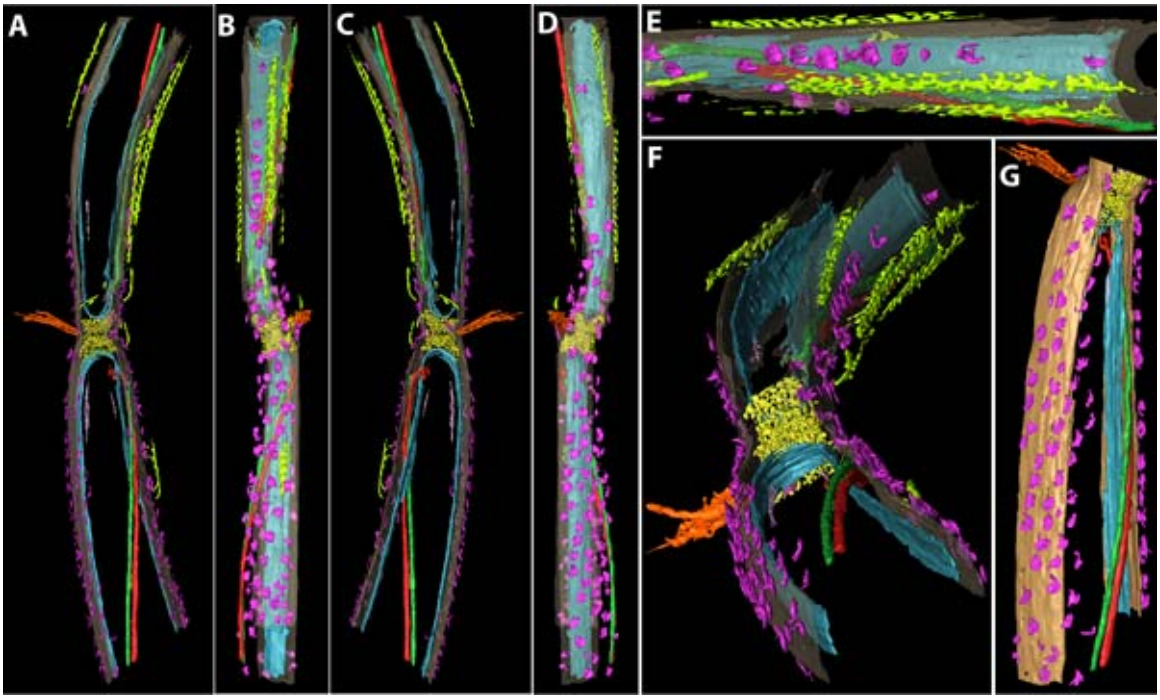

Fig. IV-3. Surface views of a connected cell

A-D. Four side views of a connected cell (cell #2), incrementally rotated by 90˚. E. A magnified view of the top cell showing the nearly matched winding of the hook arcades over the flagella. F. Oblique view similar to panel A showing multiple arcades around the cell, including one pair over the flagella and two others not above flagella. G. Oblique view similar to panel D, showing the only instance in segmented cells where the surface bowls appeared in helical rows around the cell.

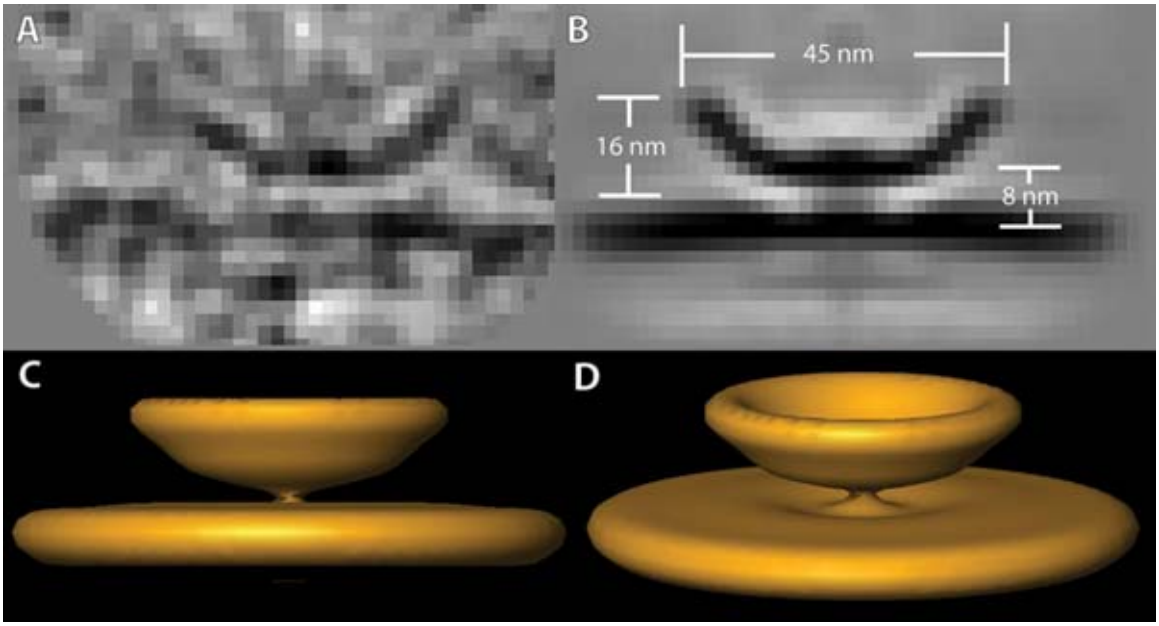

Fig. IV-4. Surface bowls

A. Axial section through the 3-D reconstruction of a single surface bowl. B. Axial slice through the symmetrized average of many bowls. C–D. Different views of an isosurface of the symmetrized average.

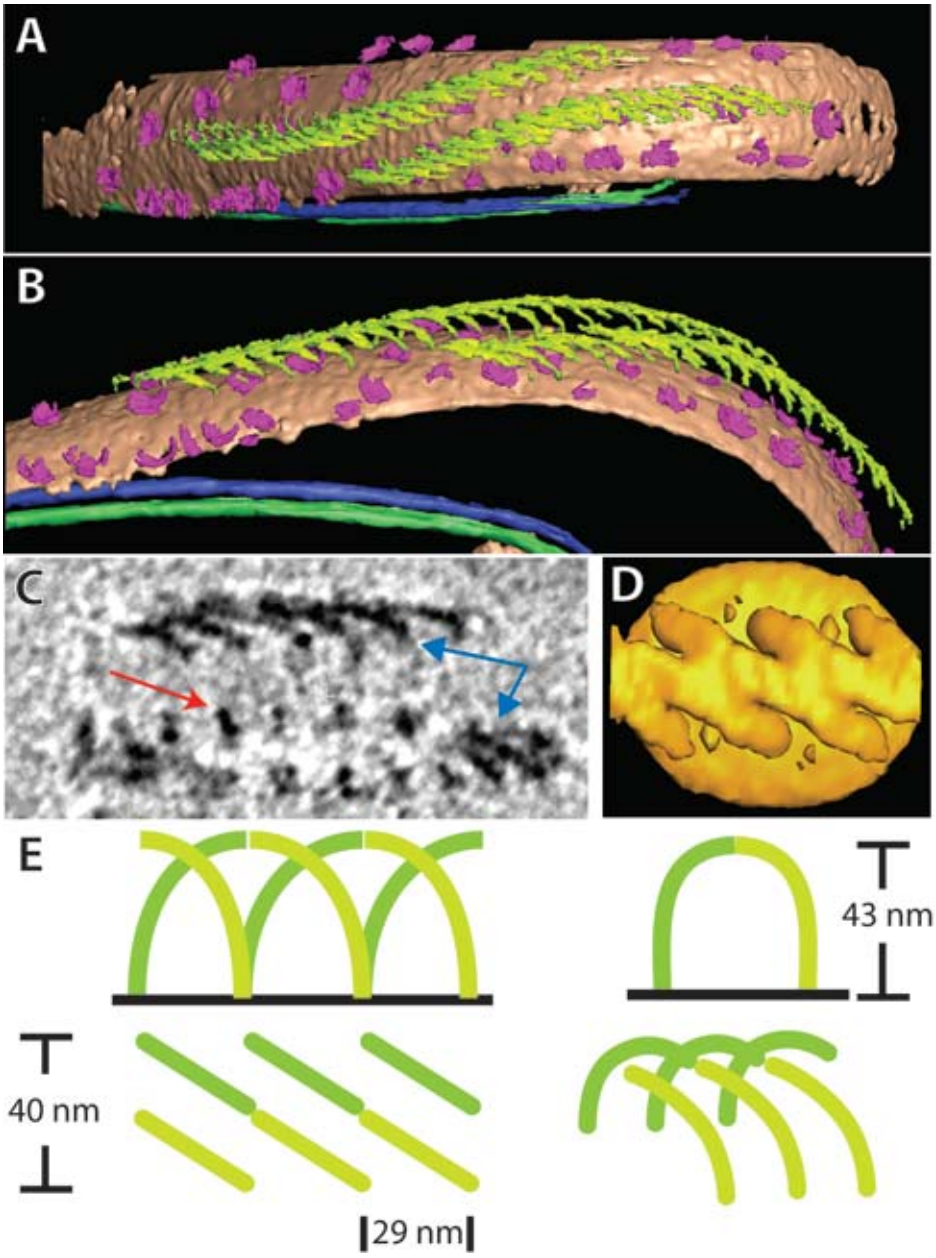

Fig. IV-5. The Hook Arcade

A. Top view of cell #3 (partially lysed) showing a pair of hook arcades. B. Oblique view of the same hook arcades. C. 4 nm section through the 3-D reconstruction, showing individual hook pillars (red arrow) and elsewhere the top of the arcade (blue arrows). D. A top view of the two-fold, symmetrized average of several hook arcade sections. E.

Cartoon drawing of the individual hooks that constitute an arcade. A hook arches over and abuts an opposite hook two pillars down.

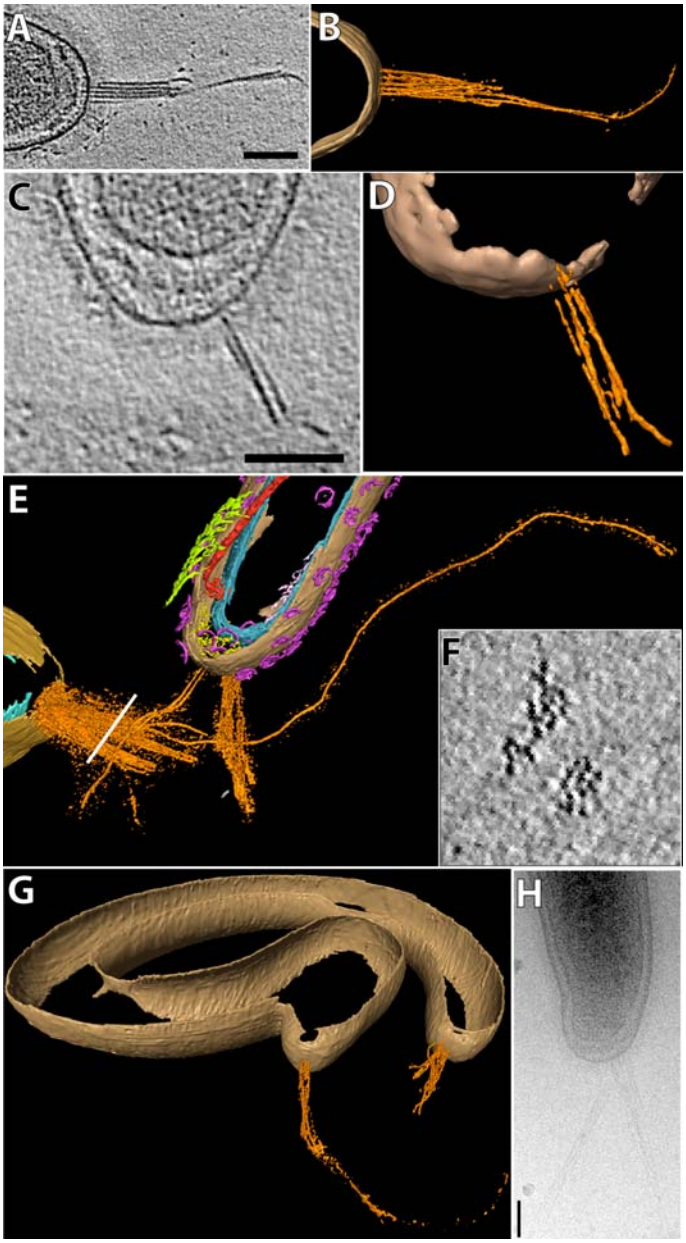

Fig. IV-6. Polar Fibrils

A. 2 nm section through the tip of cell #4, showing several fibrils extending from the tip. B. 3-D view of cell #4, showing an isosurface of the fibrils and a manual segmentation of the outer membrane. C. 2 nm section through the tip of cell #3, showing what appears to be continuous density from the fibrils through the periplasmic cone to the inner

membrane. D. 3-D view of cell #4 as in panel B. E. Isosurface of the fibrils extending from cell #1 (top) and from an additional cell (#1a, lower left) present in the same reconstruction. The fibrils in cell #1a are much more numerous, touch each other, and one fibril is ~ 1.6 μm long. F. Cross section through the bundle of fibrils from cell #1a taken at the white line in panel E. The individual fibrils are ~ 6 nm thick. G. 3-D view of cell #5, showing fibrils extending from both tips. H. Projection image of the tip of cell #6, showing forked fibrils. (All scale bars are 100 nm.)

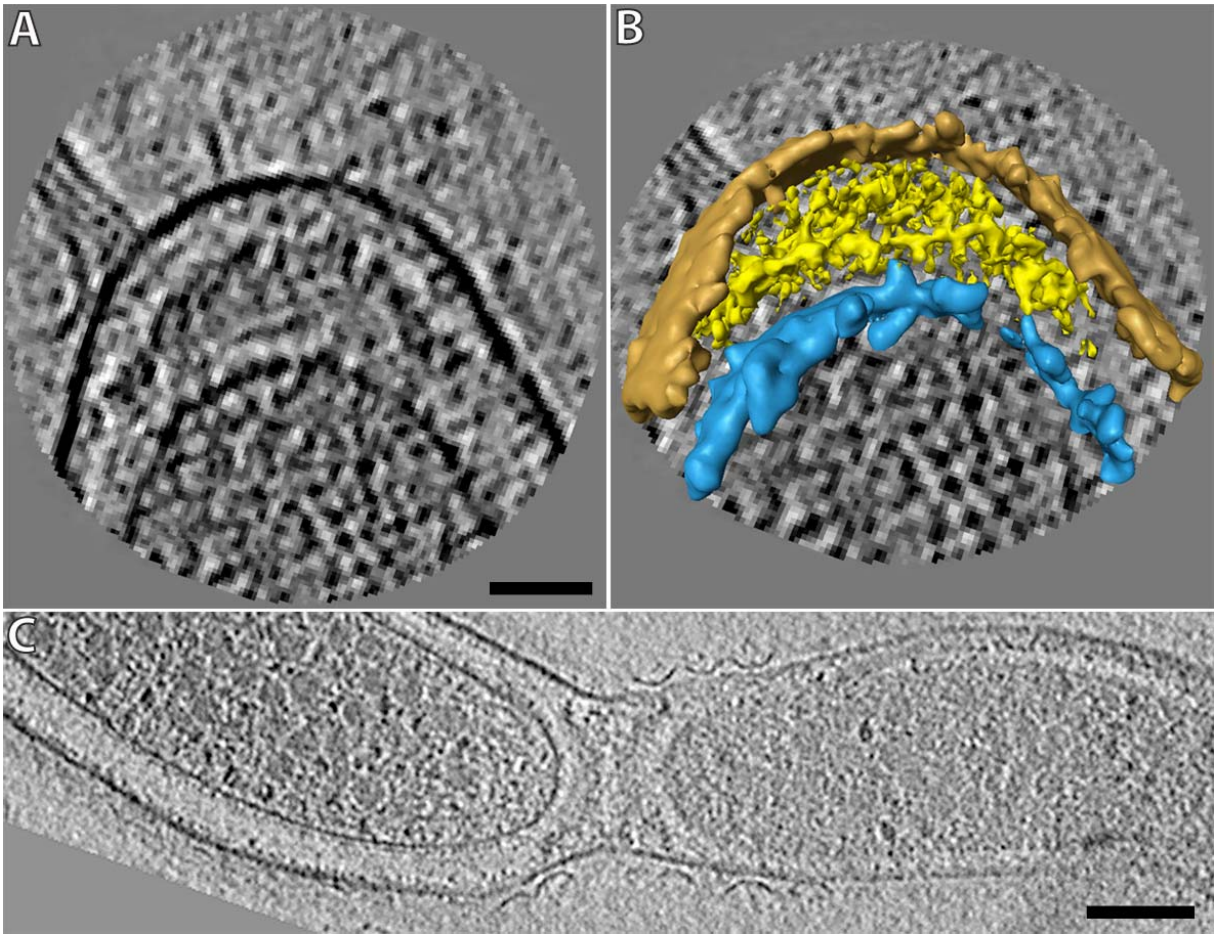

Fig. IV-7. Periplasmic cone

A. 2 nm section through the periplasmic cone of cell #1. (Scale bar is 40 nm.) B. 3-D view of cell #1, showing an isosurface of the periplasmic cone and manual segmentations of the outer and inner membranes. C. 6 nm section through two connected cells (#7 left and #7a right). The two periplasmic cones abut each other in the shape of an hourglass. Cell #7 was also remarkable because its cytoplasm was packed with ~ 30 nm wide, spherical bodies. (Scale bar is 100 nm.)

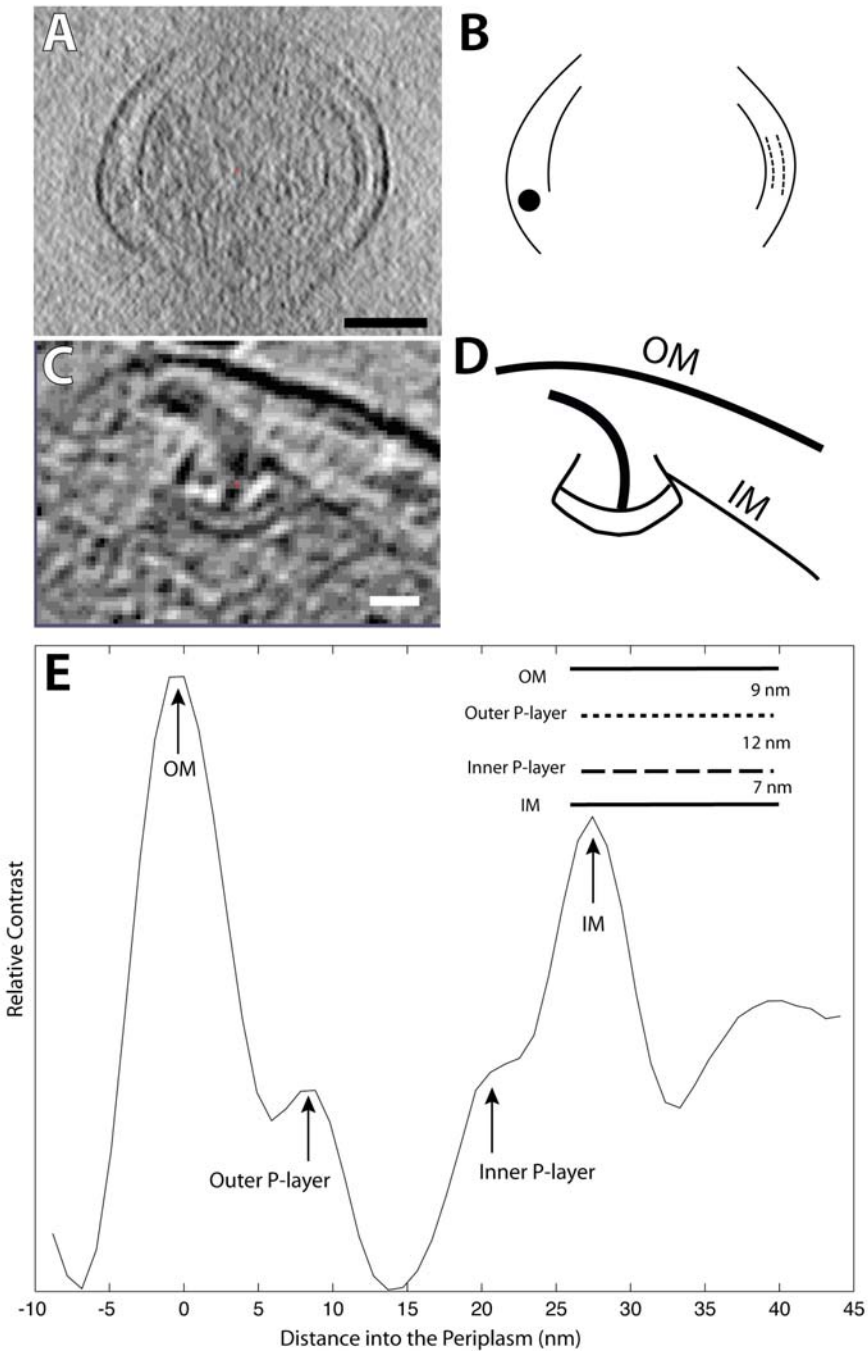

Fig. IV-8. Inner and outer periplasmic layers

A. 10 nm section through cell #8, showing two distinct periplasmic layers on the right side. The flagellum is at the bottom left. (See Sup. Mov. IV-4. Scale bar is 100 nm.) B. Cartoon guide to panel A. C. 10 nm section through a region around the flagellar motor,

showing the bulge of the periplasm near the motor. (Scale bar is 20 nm.) D. Cartoon guide to panel C. E. Average density of the periplasm as a function of distance into the cell from the outer membrane. The outer and inner periplasmic layers ("P-layers") are manifest by the smaller peaks between the two membranes.

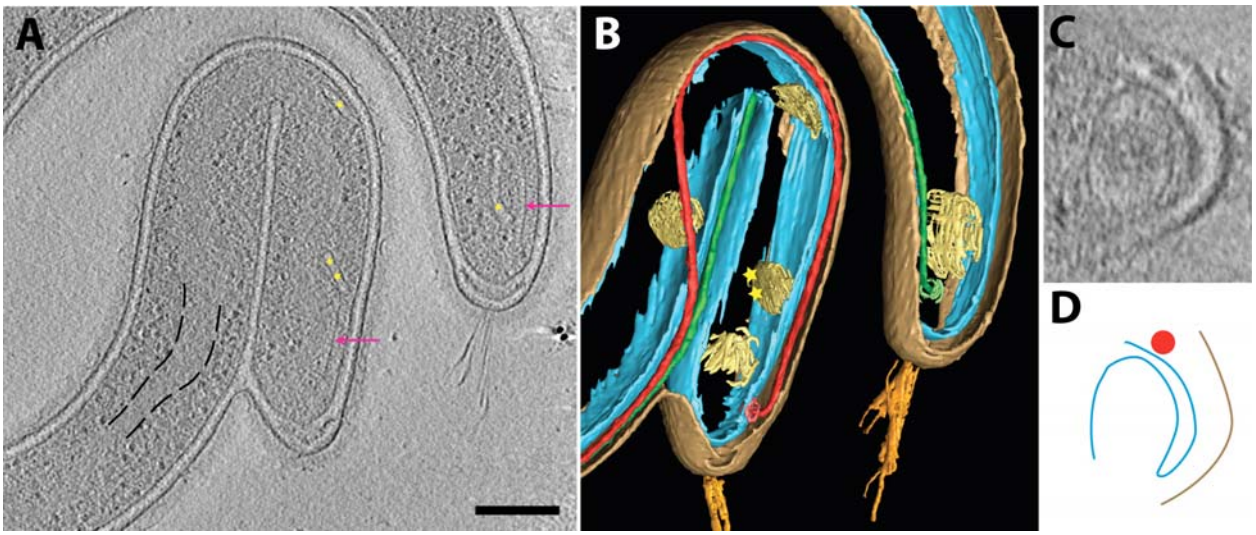

Figure 9. Cytoplasmic structures

A. 6 nm section through cell #5 showing internal membranes (gold stars), probable chemotaxis receptor arrays (pink arrows), and ribosome-excluding regions (one example region delineated by black dashed lines). (Scale bar is 200 nm.) B. Manual segmentation of cell #5. The membranes in the cytoplasm are flattened sacs near the inner membrane. C. Inclined, interpolated 6 nm section through the membrane sac marked with double gold stars in panels A and B that appears to be an infolding of the inner membrane. D. Cartoon tracing of the membranes in panel C.

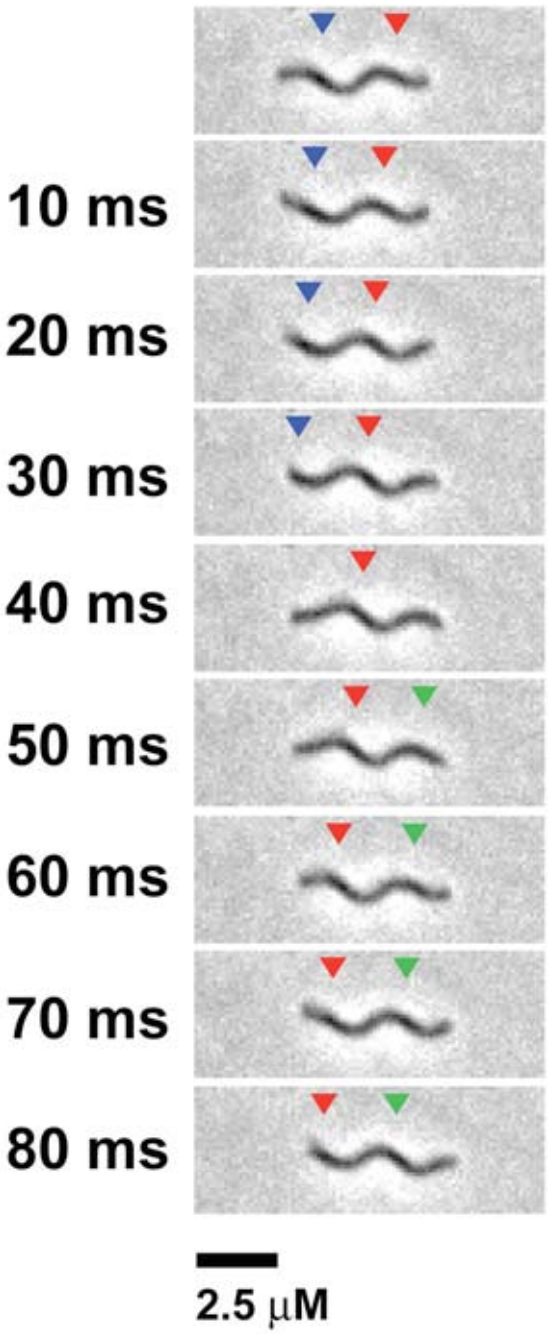

Fig. IV-10. A swimming *T. primitia* cell

Swimming cells were observed in a light microscope. Sequential frames of a single cell are pictured, showing that the cell maintains a constant helical shape as it swims. Arrows point to cell segments located in the focal plane. The cells swim at 12 μm/s in this buffer. See also Supp. Movie IV-5 for the complete movie.

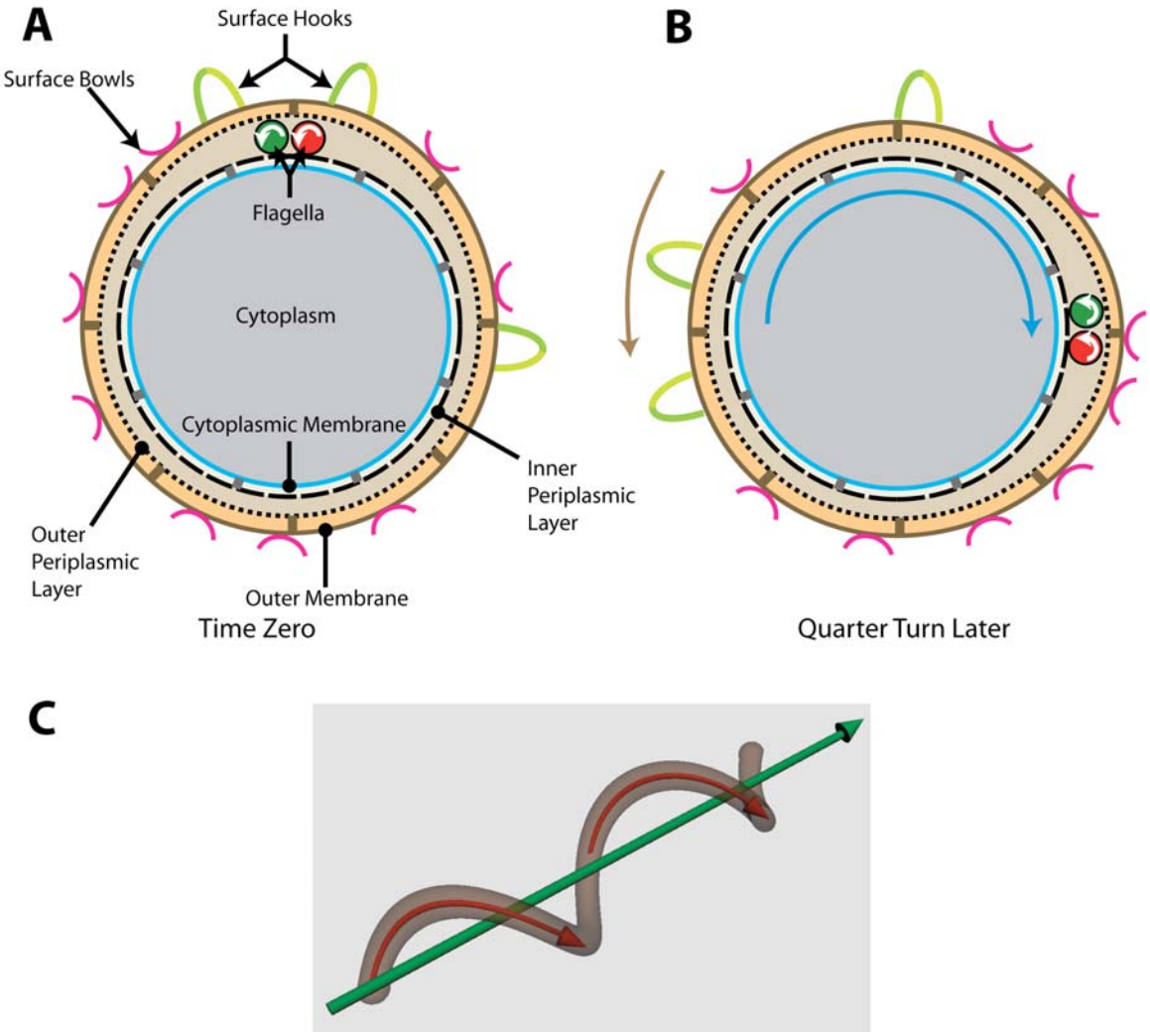

Fig. IV-11. Model of *T. primitia* ultrastructure and motility

A. Schematic cross section with labeled components at an imagined point (time "zero") when the flagella are rotating counter-clockwise (white arrows). The relative sizes of the cell thickness and the surface structures are to scale. B. Same cross section a quarter turn later. C. Oblique view of whole cell. Friction between the flagella and the outer sheath (outer periplasmic layer and outer membrane) may cause the outer sheath to rotate counter-clockwise (brown arrow). In contrast, the protoplasmic cylinder (the inner

periplasmic layer and inner membrane) must remain approximately fixed with respect to the flagella because they are attached at the position of the motor. Friction of the outer sheath against the environment may then cause the entire cell to roll clockwise (blue arrow). The helical cell would then drill itself forward like a corkscrew (red and green arrows).